SURFACE AND INTERFACE ANALYSIS
Surf. Interface Anal. 2001; **32**: 228–235

SIA

Adsorbate-induced reconstructions and nanostructures on high-index copper surfaces†

A. T. S. Wee,* Y. P. Guo, K. C. Tan, H. Q. Wang, T. K. Leong and C. H. A. Huan

Department of Physics, National University of Singapore, Kent Ridge, Singapore 119260

Received 23 October 2000; Revised 12 November 2000; Accepted 12 November 2000

High-index copper surfaces generally show a strong tendency to reconstruct, forming one- or even two-dimensional periodic nanostructures. In this paper, a survey will be presented of the various oxygen-induced reconstructions reported on high-index copper surfaces. In particular, the reconstructions of the Cu(210)–O system are presented, as revealed by low-energy electron diffraction (LEED) and scanning tunnelling microscopy (STM). The adsorption of oxygen leads to a series of $(n \times 1)$ $(n = 4, 3, 2)$ surface reconstructions, the Cu(210)–(2×1)O structure being the most stable. Quantitative LEED analysis confirms an added row model comprising Cu—O—Cu rows along the [001] direction on the topmost layer with oxygen at the long bridge sites. A range of faceting behaviour and nanostructure formation is also observed for the Cu(210)–O and Cu(210)–Br systems, and compared with other high- and low-index Cu surfaces. Copyright © 2001 John Wiley & Sons, Ltd.

KEYWORDS: high index; copper; reconstructions; LEED; STM

INTRODUCTION

The structures of crystalline surfaces are modified by the adsorbates, often by minor rearrangements to accommodate the adsorbate atoms but sometimes by major restructuring of the surface. Rough or high-Miller-index surfaces in particular appear to exhibit high adatom mobility, and coordinatively unsaturated surface atoms move easily towards new and more bulk-like equilibrium positions.[1] Restructuring occurs in order to maximize the bonding and stability of the adsorbate–substrate complex. It is driven by thermodynamic processes and occurs when the stronger adsorbate–substrate bonds that form compensate for the weakening of bonds between the substrate atoms, which is an inevitable accompaniment to the chemisorption-induced restructuring process. In this paper, we first review the structures formed on high-Miller-index copper surfaces under the influence of adsorbates, in particular oxygen. We then focus on the Cu(210) surface and the structure of its clean surface and adsorbate-induced reconstructions.

The structure of oxygen chemisorption reconstructions on low-index Cu surfaces are already well known.[2] Oxygen chemisorption on both Cu(110) and (100) surfaces leads to substantial reconstruction of the topmost Cu atom layer. Both reconstructions appear to receive stability from being able to accommodate O–Cu–O building blocks, of the sort needed to construct bulk Cu_2O.[3] The oxygen atoms are fourfold coordinated, but are not quite centred in the Cu tetrahedra. Each oxygen atom achieves a four-coordinate status with reasonable O–Cu bond lengths of 1.85–1.90 Å. On Cu(100), oxygen induces a $(\sqrt{2} \times 2\sqrt{2})R45°$–O reconstruction involving the removal of every fourth Cu[001] atom row. For Cu(110), the (2×1)–O phase is an 'added row' structure with every other Cu[001] atom row absent, and oxygen atoms occupy nearly collinear long-bridge sites in the added rows to form O–Cu–O chains. The Cu(210) surface also displays the (2×1)O added row structure, but with a larger inter-row spacing.[4] The Cu(410) surface is known to be particularly stable and faceting of Cu(100) vicinals to {410} planes in the presence of oxygen adsorbates has been well documented.[5–13] The Cu(610)[12] and Cu(810)[10] surfaces also form {410} and {100} facets. The highly stable oxygen-covered Cu(410) surface is believed to have a missing row at the bottom of each atomic step,[12] and is analogous to the Cu(100)$(\sqrt{2} \times 2\sqrt{2})R45°$–O structure, which has a missing row for every fourth Cu[001] atom row. For the Cu(511) surface, exposure to oxygen causes the formation of {410} and {311} facets.[11,13] In contrast to these terrace-driven types of surface reconstructions, the Cu(211) forms a double step reconstruction that is entirely governed by the step edges.[14] As can be seen above, most high-index Cu surfaces do not form stable reconstructions, but rather facet when exposed to oxygen. This work shows that Cu(210) can form a stable (2×1)–O reconstruction and other metastable $(n \times 1)$–O reconstructions, but can also form a range of facet structures under certain conditions of oxygen exposure and annealing.

*Correspondence to: A. T. S. Wee, Department of Physics, National University of Singapore, Kent Ridge, Singapore 119260.
E-mail: phyweets@nus.edu.sg
†Paper presented at APSIAC 2000: Asia–Pacific Surface and Interface Analysis Conference, 23–26 October 2000, Beijing, China.

DOI: 10.1002/sia.1043

EXPERIMENTAL AND COMPUTATIONAL METHODS

The quantitative current–voltage low-energy electron diffraction (IV-LEED) and scanning tunneling microscopy (STM) experiments were performed in separate ultrahigh vacuum systems. The IV-LEED measurements were carried out in a μ-metal shielded ultrahigh vacuum (UHV) chamber equipped with a combined turbomolecular and titanium sublimation pump. The base pressure of this UHV system was $<7 \times 10^{-10}$ mbar. The polished Cu(210) single crystal with a diameter of 12 mm and thickness of 2 mm was mounted on a four-axis precision manipulator, which allowed optimum alignment for normal incidence of electron beam and appropriate thermal treatment. Before the LEED measurements, the Cu(210) crystal was cleaned by repeated cycles of Ar^+ bombardment for 30 min (1.5 keV, 18 μA) followed by subsequent annealing (900 K, 30 min). Sample cleanliness was checked by the sharpness of the (1×1) spots. The LEED intensities for 14 beams were recorded at room temperature and at normal incidence using a computerized system consisting of a four-grid LEED optics, a slow-scan CCD camera and an analogue/digital data acquisition system. The energy range of the spectra was 28–300 eV, giving a cumulative energy range of 1360 eV. The background subtraction for each spot was performed by the same procedure as described in Ref. 15. Moreover, the intensity was normalized to the beam current at the respective energy. Several sets of independent data were measured and compared among the different measurements, yielding very small deviations between these experimental curves. The resulting I/V curves of the equivalent spots then were averaged and smoothed with a three-point smoothing function before they were used for structure determination.

The IV-LEED calculations were performed using programs from the Barbieri/Van Hove Symmetrized Automated LEED [or SATLEED] package.[16] For Cu(210) with atomic layer spacings of <1.0 Å (0.807 Å), the renormalized forward-scattering (RFS) perturbation does not converge well due to the divergences in the underlying LEED theory. Thick composite layers therefore were organized using 10 sublayers in the composite layer and the bulk interlayer vector was doubled by considering alternate bulk layers while doing layer stacking by RFS.[17] This methodology has been applied previously in studies of adsorption on high-Miller-index crystal surfaces.[18]

The STM experiments were conducted in an ion and turbomolecular pumped UHV system with base pressures of better than 1×10^{-10} mbar. The system is equipped with an Omicron room-temperature STM microscope stage, Omicron rearview LEED optics and Omicron CSA analyser and twin anode x-ray source for XPS measurements. Samples were mounted on a Ta sample plate and held in position with 0.25 mm diameter Ta wire spot-welded to the sample plate. The polished Cu(210) crystal was cleaned by repeated cycles of Ar^+ sputtering (1.5 keV, 30 min) and annealing (900 K, 30 min) until good (1×1) LEED patterns were observed and XPS was free of signals due to surface contaminants. Sample heating was effected by radiative emission from a tungsten filament immediately behind the sample plate. A chromel alumel thermocouple measured the temperature of the sample support plate.

The STM tips were prepared by electrochemically etching polycrystalline 0.25 mm diameter tungsten wire in 2 M NaOH solution. The tips were degassed by heating at 600 ° C before use. The piezo drives in the microscope were calibrated from atomically resolved STM images of Si(111)-(7×7) and Ni(110)-(1×1). In the oxygen uptake experiments, oxygen was introduced into the UHV chamber via a precision leak valve and the pressure was measured using an uncalibrated ion gauge. Oxygen exposures are reported in Langmuir ($1\ \mathrm{L} = 1 \times 10^{-6}$ Torr·s).

CLEAN Cu(210) SURFACE STRUCTURE

The fcc Cu{210} planes have a primitive surface unit mesh that is oblique, with parameters $a = 0.441$ nm, $b = 0.361$ nm and $\theta = 114.098°$ as shown in Fig. 1, where the shaded atoms represent the top layer of copper atoms. The (210) surface may be regarded as having the maximum step density in the [001] zone, comprising {100} terraces two atom rows wide separated by monatomic {110} steps. It therefore occupies a pivotal position between the low-index (100) and (110) planes and the higher index (n10) planes that contain wider terraces. This more open structure accounts for the higher reactivity observed on the Cu(210) surface.[19,20]

When sharp (1×1) LEED patterns are observed, STM images of the clean Cu(210) show a relatively flat surface with wide terraces and monatomic steps. The dynamic nature of the step edges is highlighted by the two subsequently recorded STM images in Fig. 2 of the same area. It can be seen that the step edges change position and shape within a time scale of minutes at room temperature. Previous experience with the Omicron STM instrument tells us that this cannot

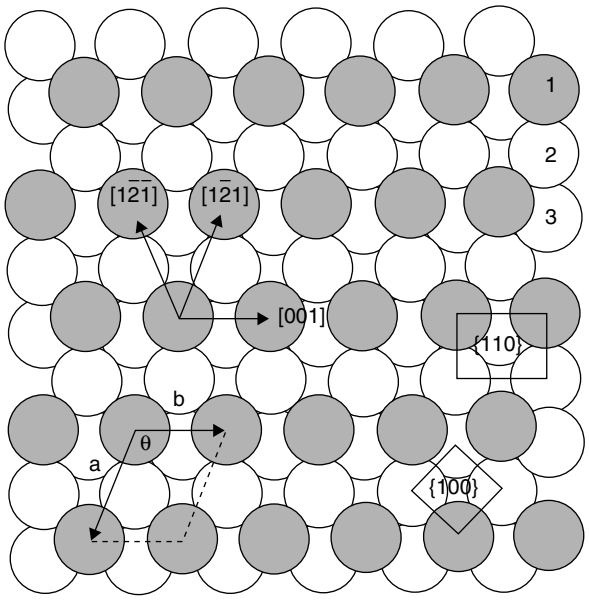

Figure 1. Schematic of the Cu(210) surface showing the oblique primitive cell with $a = 4.41$ Å, $b = 3.61$ Å and $\theta = 114°$. A {100} terrace and {110} step are highlighted. Numbers indicate first, second and third layer atoms; the first layer of Cu atoms are shaded for clarity.

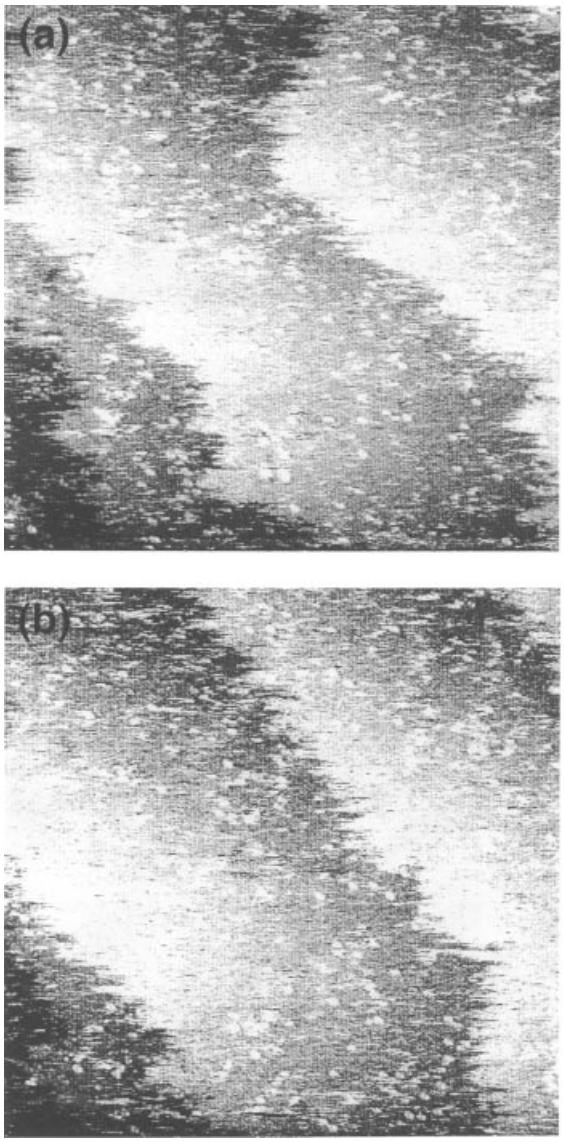

Figure 2. The 400 × 400 Å^2 images of the same area of clean Cu(210) recorded 5 min apart at $V_B = -20$ mV and $I_T = 3.0$ nA. Note the relative changes in the three monatomic step profiles due to the dynamic detachment and reattachment of Cu atoms from the step edges.

be due to instrumental drift on this time scale. Hence, the step fluctuations on Cu(210), as in the case of Cu(110), are interpreted as the displacement of edge atoms by the release and recondensation of Cu atoms from step edges. The Ibach group have studied surface self-diffusion on Cu(100)[21] and reported that the mass transport is attachment–detachment-limited at the steps because surface vacancies are primarily responsible for mass transport between step edges. It will be shown later that the Cu(210) step edges can be stabilized by chemisorbed oxygen.

For quantitative LEED analysis, the top five interlayer spacings (d_{12}, d_{23}, d_{34}, d_{45} and d_{56}) of Cu(210) were optimized to experimental data using a muffin-tin radius of 1.217 Å and a real part of inner potential 8 eV, giving a best-fit minimum R_p factor of 0.20.[17] Here, we emphasize the relaxation perpendicular to the surface, although the rearrangements parallel to the surface indicate a smoothening of the highly corrugated surface. The top three interlayer spacings of the clean reconstructed Cu(210) surface are calculated to be $d_{12} = 0.761 \pm 0.04$ Å, $d_{23} = 0.759 \pm 0.04$ Å and $d_{34} = 0.862 \pm 0.03$ Å, respectively. The corresponding relaxation percentages are $\Delta d_{12}/d_0 = -5.7 \pm 5\%$, $\Delta d_{23}/d_0 = -6.0 \pm 5\%$ and $\Delta d_{34}/d_0 = 6.8 \pm 4\%$.

Table 1. Experimental and theoretical percentage relaxations relative to bulk interlayer spacings for Cu(210)

Surface	Ref.	Δd_{12}	Δd_{23}	Δd_{34}	Δd_{45}	Δd_{56}
Cu(210)	Exp.[17]	-5.7 ± 5	-6.0 ± 5	$+6.8 \pm 4$	-3.7 ± 5	-0.5 ± 4
	MEAM[22]	−13.37	−1.42	+4.75	−2.17	—
	ECT[23]	−4.28	−6.73	+0.39	—	—

Our multilayer relaxation results for clean Cu(210) agree very well with theoretical results calculated from the semi-empirical modified embedded atom method (MEAM)[22] and equivalent crystal theory (ECT),[23] as summarized in Table 1. Both MEAM and ECT predict contractions in the first two interlayers and expansion in the third interlayer for Cu(210). The results are also consistent with experiment and theory for Al(210)[24] and Pt(210),[25] which all point to significant inward surface relaxation resulting in smoothening of the corrugated (210) surface for fcc metals. The atoms on the *rough* surface change their bulk equilibrium positions, thereby minimizing the surface free energy, maximizing coordination number within the surface layer and thus bringing about a smoother surface. This results in exposure of the deeper trough atoms. During the uptake of adsorbates, they can interact not only with the atoms in the first layer but also in the second layer, forming stable structures with high coordination numbers.

OXYGEN-INDUCED RECONSTRUCTIONS ON Cu(210)

We have performed a series of oxygen adsorption experiments on Cu(210) using LEED at substrate temperatures between 300 and 700 K. Oxygen adsorption in this temperature range results in a series of ($n \times 1$) reconstructions, namely (2 × 1), (3 × 1) and (4 × 1), as summarized by the phase diagram in Fig. 3 (details available from the author upon request). The (2 × 1) reconstruction was found to be the most stable reconstruction because annealing the (4 × 1) or (3 × 1) reconstructions invariably leads to a (2 × 1) reconstruction, which could be saturated or unsaturated, depending on the initial oxygen coverage. Figure 4(a) shows a 300 × 300 Å^2 STM image of the (2 × 1) reconstruction formed after oxygen exposure at 550 K. A well-formed (2 × 1) reconstruction corresponding to an oxygen coverage of $\theta = 0.5$ now has completely covered the surface, consistent with the good (2 × 1) LEED pattern observed. This image clearly shows the diperiodic atomic rows along the [001] direction with an inter-row spacing of 8.07 Å. The detailed Cu–O row structure has been determined by IV-LEED,[26] and surface-extended x-ray adsorption fine structure (SEXAFS).[27] We postulate that the (3 × 1) reconstruction corresponds to added rows with 2/3 or 1/3 monolayer coverage, and that the (4 × 1) reconstruction corresponds to a 1/4 monolayer coverage, as illustrated by the models in Fig. 5. Preliminary

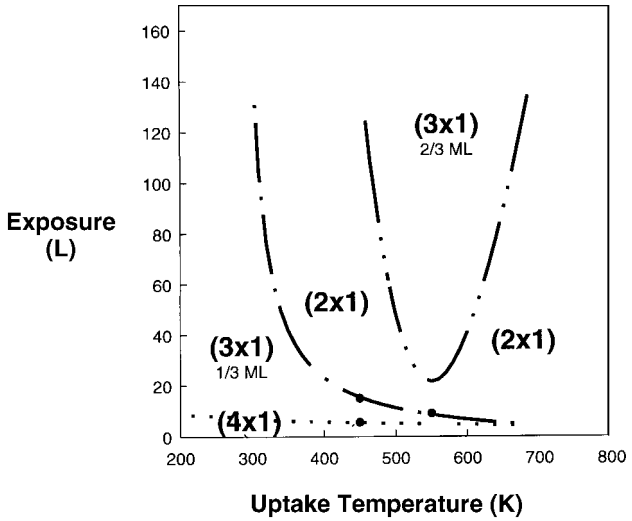

Figure 3. Phase diagram of oxygen exposure (in Langmuir) on Cu(210) determined by LEED at substrate temperatures of 300–700 K. A series of ($n \times 1$) reconstructions, namely (2×1), (3×1) and (4×1), are observed but the patterns at room temperature are rather streaky.

IV-LEED experiments for the (3×1) model support these conclusions. Such regular added row reconstructions imply the presence of relatively long-range inter-row repulsive interactions. The phase diagram (Fig. 3) shows that the maximum sticking probability of oxygen occurs at a substrate temperature of 550 K, suggesting two competing processes of oxygen trapping at Cu–O rows (dominating at lower temperatures) and oxygen desorption (dominating at higher temperatures).

Subsequent annealing of the saturated (2×1)–O reconstruction to incrementally higher temperatures resulted in a gradual depletion of Cu–O rows on the terraces. When the annealing temperature reached 820 K, Cu–O rows were observed only on the step walls. Figure 4(b) shows stabilized Cu–O rows on these step walls but no observable order on the terraces. This clearly indicates that the step edges are stabilized by oxygen. It was observed that no faceting occurred even when the (2×1)–O surface was subjected to a large oxygen exposure (180 L) at 300 K, followed by annealing for longer durations at 780 K. This is in contrast to the faceting behaviour described in the next section, and attests to the stability of the (2×1)-O phase.

The LEED patterns for the room-temperature oxygen uptake in Fig. 3 were observed to be streaky, and STM images reveal that the surface is indeed rather disordered and does not show the expected added rows. In order to understand the dynamics of the oxygen chemisorption process on Cu(210) at room temperature, STM images were recorded sequentially during oxygen exposure at room temperature. Figure 6 shows 400×400 Å^2 STM images of the same area under increasing oxygen exposures up to 18.0 L (oxygen background pressure of 2×10^{-9} mbar). At exposures as low as 1.3 L (sub-monolayer oxyen coverage), dark depressions begin to appear on the terraces. Step edges are subject to less pronounced dynamic fluctuations and no longer appear ragged; there is, however, increased irregularity. Some of

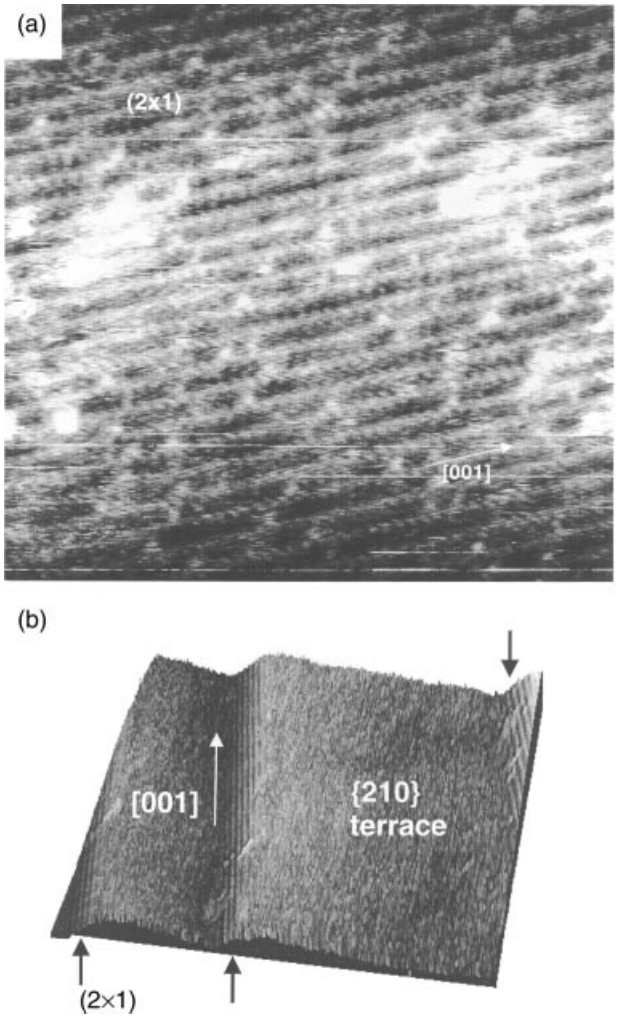

Figure 4. (a) A 300×300 Å^2 STM image of a (2×1) reconstruction after exposing Cu(210) to 5.0 L oxygen at 550 K. The image was recorded at $V_B = -0.5$ V and $I_T = 1.0$ nA. (b) Three-dimensional view of 300×300 Å^2 image ($V_B = -1.0$ V, $I_T = 1.0$ nA) taken after the surface in (a) was annealed to 820 K. The stabilized (2×1) steps along the [001] direction are indicated.

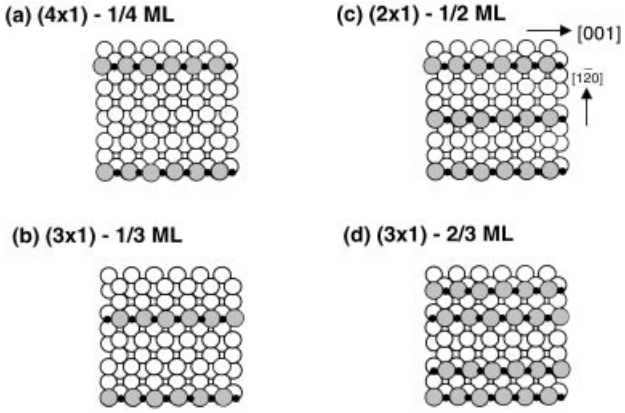

Figure 5. Models showing oxygen-induced reconstructions on Cu(210): (a) (4×1) (1/4 ML); (b) (3×1) (1/3 ML); (c) (2×1) (1/2 ML); (d) (3×1) (2/3 ML). The black spheres represent oxygen atoms and the shaded spheres balls represent the added row Cu atoms.

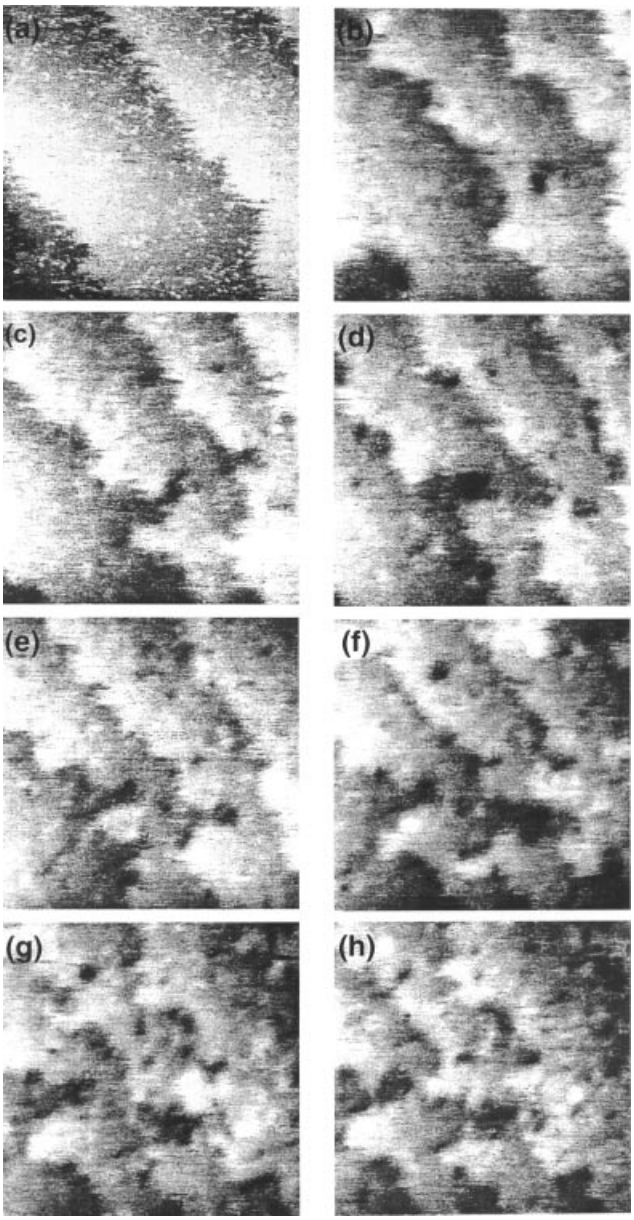

Figure 6. The 400 × 400 Å^2 images ($V_B = -20$ mV and $I_T = 2.0$ nA) of a clean surface (a) and surfaces after various room-temperature oxygen exposures: (b) 1.3 L; (c) 5.0 L; (d) 6.4 L; (e) 9.0 L; (f) 12.9 L; (g) 15.4 L; (h) 18.0 L. At 1.3 L oxygen exposure, dark depressions begin to appear on the terraces. Step edges also are subject to less-pronounced dynamic fluctuations and no longer appear ragged, indicating a stabilization of the step edges by adsorbed oxygen. There is, however, increased irregularity of the step profiles. Some of the 'inlets' along the edges eventually merge with the 'holes' on the terraces (from (c) onwards), resulting in highly irregular step edges.

the 'inlets' along the edges merge with the 'holes' on the terraces, resulting in highly irregular step edges. Subsequent images obtained by varying the sample bias suggest that these depressions are real topographical features.

Comparisons with the Cu(110)–O growth dynamics can be instructive.[28,29] On Cu(110) at 300 K, mobile Cu atoms on terraces that detach from step edges are trapped by oxygen atoms resulting from O_2 adsorption and dissociation, forming Cu–O rows along the [001] direction. At higher coverages, these rows form (2 × 1) islands that block Cu adatom diffusion and stabilize step edges. Another reaction channel then becomes competitive—that of Cu adatom generation through the formation of rectangular troughs on terraces. On Cu(210), however, no regular Cu–O rows were observed to form at 300 K. Nevertheless, the formation of irregularly shaped troughs on terraces appears to be at least as favourable as the removal of Cu adatoms from step edges. These Cu adatoms eventually form a myriad of stacked islands at higher oxygen exposures.

The stabilization of step edges along the [001] direction continues for exposures above 20 L, thereafter followed by island growth on the terraces near these step edges. The image resolution was observed to degrade during the uptake experiment due to the oxygen ambient, but subsequent reconditioning of the tip by field emission resulted in atomically resolved images of the island structures. Figure 7(a) shows a 300 × 300 Å^2 STM image after 61 L oxygen exposure at 300 K. It can be observed clearly that rectangular arrays of Cu–O islands are formed with their long edges along the [001] direction. The interconnected island arrays have varying lengths but are all ~25–30 Å wide, comprising 6–8 Cu atom rows. As with previous room-temperature STM studies of oxygen on Cu, only the Cu atoms are clearly imaged and it is not possible to ascertain the oxygen adatom positions. The long edges of the islands show missing atoms with a periodicity of two or three times the Cu–Cu distance along the [001] direction (3.61 Å).

FACETING AND SUPERSTRUCTURE FORMATION ON Cu(210)

When Cu(210) was exposed to 500 L oxygen at room temperature and annealed at 620 K for a few minutes, the LEED pattern shows additional weak spots on top of the basic (1 × 1) pattern with streaks along the [1$\bar{2}$0] direction. These weak spots indicate a larger (7 × 1) or (8 × 1) surface reconstruction, which becomes immediately apparent in the STM image of Fig. 7(b). This image shows long-range spatial self-organization along the [1$\bar{2}$0] direction, forming a striped periodic structure with mesoscopic ordering. The stripes run along the [001] direction with a grating periodicity of 28–30 Å or 6–7 Cu–O rows with a missing row between the stripes. Following Ref. 30, we refer to this as a 'supergrating'. To investigate the effect of oxygen coverage on the superstructure, lower oxygen exposures of 1.0 and 70 L were performed at 300 K, followed by brief annealing to 560–610 K. Similar but less-well-defined supergratings along the [001] direction were observed with a period of 25–30 Å. Figure 7(c) shows a 300 × 300 Å^2 image of the supergrating formed after room-temperature oxygen exposures of 1.0 L followed by brief annealing. The periodicity is similar to that observed after 500 L of oxygen exposure [cf. Fig. 7(b)], although the supergratings at lower exposures are less well formed.

The periodic supergrating for the Cu(110)–(2 × 1)O system has a larger periodicity of 60–140 Å, depending on oxygen coverage and substrate temperature.[30] The reduced

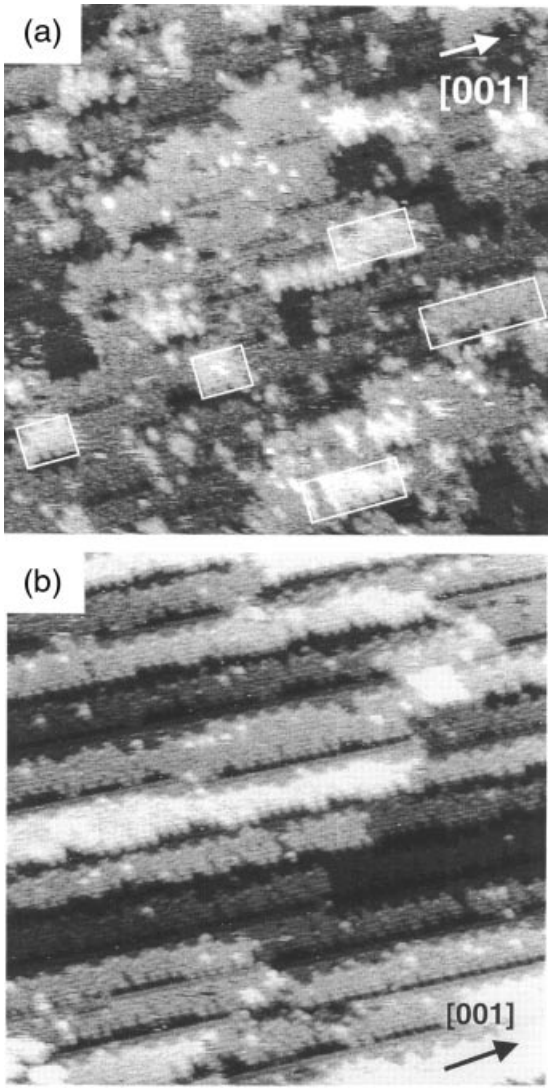

Figure 7. (a) A 300 × 300 Å^2 image ($V_B = -1.0$ V, $I_T = 0.25$ nA) after room-temperature oxygen exposure of 61 L. The tip had been reconditioned prior to STM measurements and the area scanned is not the same as in Fig. 6(h). Note that the optimized tip parameters (V_B, I_T) for the oxygen-covered surface are different from those for the clean surface. This is due to the larger atomic corrugations when oxygen is present. (b) A 300 × 300 Å^2 image ($V_B = -1.0$ V, $I_T = 0.30$ nA) image after room-temperature oxygen exposure of 500 L and subsequent annealing to 620 K for a few minutes. Analysis of corrugation profiles shows that there are one monolayer height differences between several adjacent stripes. (c) A 300 × 300 Å^2 image ($V_B = -0.5$ V, $I_T = 0.1$ nA) of Cu(210) after room-temperature oxygen exposure of 1.0 L and annealing to 560 K. It is apparent that the superstructure periodicity is similar to that observed after 500 L oxygen exposure (b), although the supergrating at 1.0 L is less well formed.

spacing of 4.03 Å between the [001] Cu–O rows on Cu(210) appears to result in narrower stripes (28–30 Å) due to larger long-range repulsive forces. Hence, we conclude that, unlike the Cu(110)–O system, the supergrating periodicity for Cu(210)–O shows no dependence on oxygen exposures of 1–500 L. At higher oxygen exposures, however, the

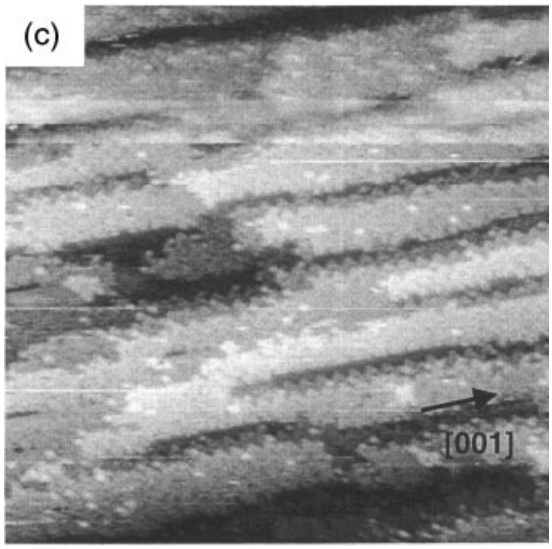

Figure 7. (*Continued*).

superstructure is several atomic layers thick due to the prior formation of multiple steps, troughs and island growth. A theoretical model is needed to explain the superstructure formation in both systems.

Unlike low-index surfaces, most high-index Cu surfaces do not form stable reconstructions but facet when exposed to oxygen. The Cu(210) surface also exhibits oxygen-induced restructuring during annealing at longer time scales, resulting in a range of superstructure and faceting behaviour.[4] Restructuring occurs in order to maximize the bonding and stability of the adsorbate–substrate complex. It is driven by thermodynamic forces and occurs when the stronger adsorbate–substrate bonds that form compensate for the weakening of bonds between the substrate atoms. The resulting structures are believed to possess the basic geometry of bulk Cu_2O.

Several trends have emerged from previous studies on oxygen-induced faceting of high-index copper surfaces. For Cu(n10) and Cu(n11) surfaces (where $n > 4$), the O/Cu(410) facet invariably forms, attesting to the extreme stability of this surface. This has been observed for Cu(810),[9,10] Cu(610),[12] Cu(16 1 1),[31] Cu(11 1 1),[9] Cu(711)[9] and Cu(511).[11,13] Other facets, of course, also form in order to maintain the overall macroscopic orientation of the surface. For the Cu(210) and Cu(211) surfaces, however (where $n < 4$), O/Cu(410) facets are not observed. The Cu(211)–O system forms several reconstructions, depending on experimental conditions.[14] In particular, highly ordered and thermally stable double-step structures are observed. For the Cu(210)–O system, there appears to be two competing pathways that result in either stable Cu(210)–($n \times 1$)O reconstructions or a series of faceting behaviour.[4] The Cu(210) facet step edges initially align along the [001] direction and eventually form triangular facet structures with monoatomic steps along the [001], [1$\bar{2}$1] and [1$\bar{2}\bar{1}$] directions. A possible driving force for these observed reconstructions is the minimization of the surface free energy, and total energy calculations are needed for further understanding of these systems.

BROMINE-INDUCED NANOSCALE STRUCTURES ON Cu SURFACES

There is much recent interest in adsorbate–substrate systems that spontaneously form structures with mesoscopic periodicity.[32] Such nanostructures could possess novel transport and magnetic properties and could be used in nanoscale selective-area deposition. Two systems that display such behaviour will be presented here: the Cu(210)–Br and Cu(100)–Br systems. Note that Br-induced reconstructions are different from oxygen-induced reconstructions due to the stronger ionic nature of the Br–Cu bond.

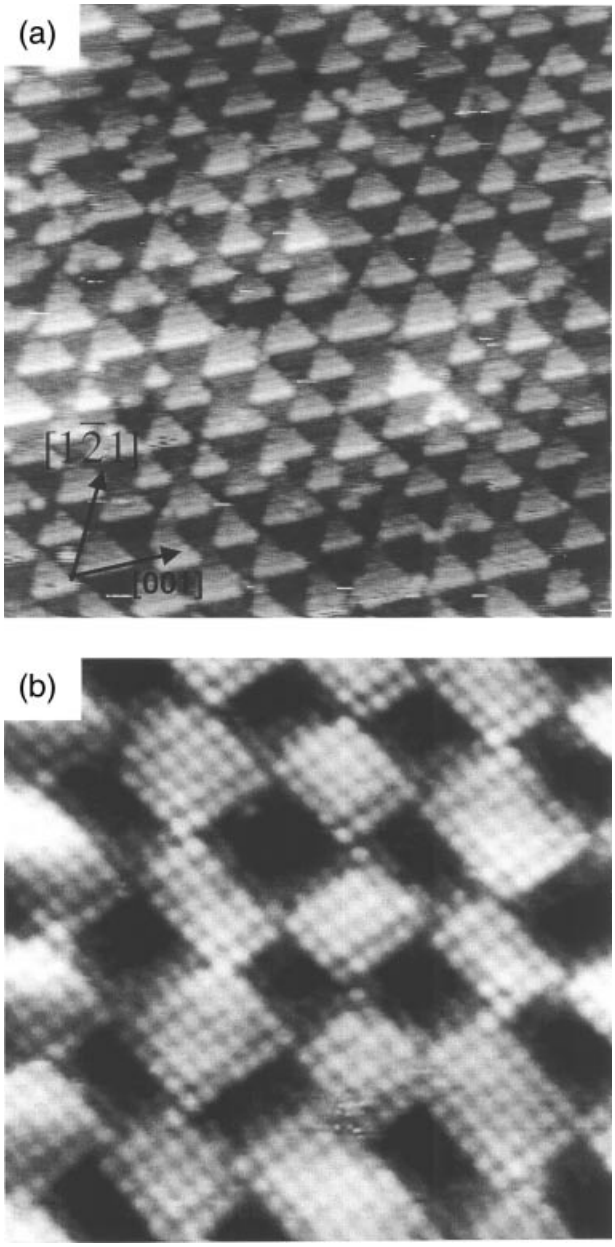

Figure 8. (a) A 200 × 200 Å^2 image of the triangular checkerboard on Cu(210) recorded at $V_B = -1.0$ V and $I_T = 0.1$ nA. Several monatomic step edges are highlighted by dotted lines. (b) A 100 × 100 Å^2 image of the Br–Cu(100) square chessboard pattern.

When Cu(210) was dosed with Br at room temperature and subsequently annealed to 610 K for a few minutes, a mesoscopic triangular checkerboard was observed [Fig. 8(a)].[33] The basic triangular unit comprises four or five atom rows (made up of 10 or 15 atoms, respectively) in the {210} plane, with edges of the triangle along the [001], [1$\bar{2}$1] and [12$\bar{1}$] directions. The triangular checkerboard pattern merges with the adjacent stepped substrate planes, indicating that the triangles comprise Cu atoms. This hypothesis is also supported by scanning tunnelling spectroscopy (STS) data, which show little differences between spectra of atom sites on the triangles and in the depressions (inverted triangles). Hence, Br is believed to have etched the Cu(210) surface to leave the mesoscopic checkerboard structure, which reflects {210} symmetry.

For the Cu(100)–Br system, a corresponding mesoscopic chessboard structure is observed.[34] Figure 8(b) shows this chessboard pattern of Br atoms on Cu(100) after bromine dosing followed by a 10 min anneal to 100 °C. Under these conditions, no desorption of Br was observed. The step edges are oriented along the {100} directions, reflecting the Cu(100) substrate symmetry, and the 'white' Br squares have a local c(2 × 2) reconstruction. It appears that in this system, the adsorption and etching due to bromine provide a mechanism for the development of strain within the mesoscopic islands, thus limiting their island size. A theory is still needed to explain the stability of these interesting nanostructures.

CONCLUSION

The oxygen-induced reconstructions on Cu(210) are presented and compared with those on other high- and low-index copper surfaces. The adsorption of oxygen leads to a series of $(n \times 1)$ $(n = 4, 3, 2)$ surface reconstructions, the Cu(210)–(2 × 1)O structure being the most stable. Quantitative LEED analysis confirms an added row model comprising Cu–O–Cu rows along the [001] direction. Under certain conditions, another reaction pathway becomes favourable, leading to a series of superstructure and faceting behaviour. Novel nanostructure formation in the Cu(210)–Br and Cu(100)–Br systems is also compared.

REFERENCES

1. Somorjai GA. *Introduction to Surface Chemistry and Catalysis*. Wiley: New York, 1994; 412 ff.
2. Besenbacher F, Norskov JK. *Prog. Surf. Sci.* 1993; **44**: 5, and references therein.
3. Liu W, Wong KC, Zeng HC, Mitchell KAR. *Prog. Surf. Sci.* 1995; **50**: 247.
4. Wee ATS, Foord JS, Egdell RG, Pethica JB. *Phys. Rev. B*. 1998; **58**: R7548.
5. Berndt W. *Z. Naturforsch.* 1967; **A22a**: 1655.
6. Trepte L, Menzel-Kopp C, Menzel E. *Surf. Sci.* 1967; **8**: 223.
7. Perdereau J, Rhead GE. *Surf. Sci.*1971; **24**: 555.
8. Legrand-Bonnyns E, Ponslet A. *Surf. Sci.* 1975; **53**: 675.
9. Boulliard JC, Domange JL, Sotto M . *Surf. Sci.* 1986; **165**: 434.
10. Lloyd GW, Woodruff DP. *Surf. Sci.* 1993; **285**: L503.
11. Reiter S, Taglauer E. *Surf. Sci.* 1995; **367**: 33.
12. Knight PJ, Driver SM, Woodruff DP. *J. Phys.: Condens. Matter* 1997; **9**: 21.
13. Walko DA, Robinson IK. *Phys. Rev. B* 1999; **59**: 15446.
14. Witte G, Braun J, Nowack D, Bartels L, Neu B, Meyer G. *Phys. Rev. B* 1998; **58**: 13224.

15. Narloch B, Menzel D. *Surf. Sci.* 1995; **421/413**: 562.
16. Barbieri A, Van Hove MA. http://electron.lbl.gov/leedpack/
17. Guo YP, Tan KC, Wee ATS, Huan CHA. *Surf. Rev. Lett.* 1999; **6**: 819.
18. Narloch B, Held G, Menzel D. *Surf. Sci.* 1995; **340**: 159.
19. Wee ATS, Lin J, Huan ACH, Loh FC, Tan KL. *Surf. Sci.* 1994; **304**: 145.
20. Chen AK, Masel R. *Surf. Sci.* 1995; **343**: 17.
21. Hannon JB, Klunker C, Giesen M, Ibach H, Bartelt NC, Hamilton JC. *Phys. Rev. Lett.* 1997; **79**: 2506.
22. Wan J, Fan YL, Gong DW, Shen SG, Fan XQ. *Model. Simul. Mater. Sci. Eng.* 1999; **7**: 189.
23. Rodriguez AM, Bozzolo G, Ferrante J. *Surf. Sci* 1993; **289**: 100.
24. Adams DL, Jensen V, Sun XF, Vollesen JH. *Phys. Rev. B* 1988; **38**: 7913.
25. Zhang XG, Van Hove MA, Somorjai GA, Rous PJ, Tobin D, Gonis A, Maclaren JM, Heinz K, Michl M, Lindner H, Muller K, Ehsasi M, Block JH. *Phys. Rev. Lett.* 1991; **67**: 1298.
26. Tan KC, Guo YP, Wee ATS, Huan CHA. *Surf. Rev. Lett.* 1999; **6**: 859.
27. Polcik M, Haase J, Ondrejcek M, Petersen JH. *Surf. Sci.* 1998; **413**: 580
28. Coulman DJ, Wintterlin J, Behm RJ, Ertl G. *Phys. Rev. Lett.* 1990; **64**: 1761.
29. Jensen F, Besenbacher F, Laesgaard E, Stensgaard I. *Phys. Rev. B* 1990; **41**: 10233.
30. Kern K, Niehus H, Schatz A, Zeppenfeld P, Goerge J, Comsa G. *Phys. Rev. Lett.* 1991; **67**: 855.
31. Boulliard JC, Cohen C, Domange JL, Drigo AV, L'Hoir A, Moulin J, Sotto M. *Phys. Rev. B* 1984; **30**: 2470.
32. Brune H, Giovannini M, Bromann K, Kern K. *Nature* 1998; **394**: 451.
33. Wee ATS, Fishlock TW, Dixon RA, Foord JS, Egdell RG, Pethica JB. *Chem. Phys. Lett.* 1998; **298**: 146.
34. Fishlock TW, Pethica JB, Egdell RG. *Surf. Sci.* 2000; **445**: L47.